IN SITU RADIOGRAPHY OF THE METAL FOAMING PROCESSES: A QUANTITATIVE ANALYSIS.

A. Myagotin[*a], L. Helfen[*a,b], J. Banhart[**c], T. Baumbach[*a]

[a]Institut für Synchrotronstrahlung (ISS/ANKA), Forschungszentrum Karlsruhe, Eggenstein-Leopoldshafen, Germany

[b]European Synchrotron Radiation Facility, Grenoble, France

[c]Hahn-Meitner-Institut (HMI), Berlin, Germany

ABSTRACT

Methods for evaluation of series of projection images by quantitative image analysis have been developed and applied to the investigation of metal foaming processes by *in-situ* real-time radiography.

In-situ radiography allows one to image the temporal structure evolution during the foaming process and has been applied [1–5] to yield detailed information about metal foaming by the powder-metallurgical production method. Internal structural changes such as bubble expansion, structural coarsening, bubble coalescence, collapse and drainage could be observed non-destructively and investigated qualitatively.

In-depth statistical evaluation of two-dimensional (2d) projection image sequences was hardly ever performed up to now for the study of metal foams. In this paper we report different methods for the quantitative analysis of 2d projection image sequences which allow us to compare characteristic statistical properties of the temporal structure evolution during foaming. In particular, we will present a quantitative evaluation procedure of *coalescence rates*. Furthermore, from the so-called *velocity field* we will conclude on the evolution of the local expansion rates.

From the technological point of view, the new methods permit the quantitative study of the influence of foam processing conditions (*e.g.* temperature selection) and precursor properties (*e.g.* precursor material and pre-treatment) which influence the foaming process.

Keywords: metallic foam, quantitative image analysis, coalescence rate, foam expansion

[*]Email: [anton.myagotin, lukas.helfen, tilo.baumbach]@iss.fzk.de; [**]Email: banhart@hmi.de

1. INTRODUCTION

Metal foams have become a promising material for industrial needs. They permit manufacture of rather inexpensive light-weight components with wide application range, *e.g.* impact/energy absorbers, light-weight constructions and vibration dampers [6, 7].

A control over the foam manufacture process is required for a reproducible production of foams with given properties. This challenge is inseparably connected with a fundamental understanding of the foaming process which includes both physical and technological aspects.

Formation of metal foams is of complex nature. It consist of several mechanisms running in parallel, such as pore inflation, structural rearrangement, coalescence or drainage. Moreover, the metal foam itself is an inhomogeneous, opaque, chemically reactive material, what makes its investigation a rather complicated task.

Especially the investigation of the kinetics of metal foam evolution is difficult. It has been shown that *in-situ* x-ray radiography allows one to obtain insight into foaming metals [1–5]. However, an investigation of foam behaviour by means of *manual* evaluation of statistical material characteristics by 2d projection radiography is evidently prone to errors and tedious. An automated analysis is highly desirable since it could vastly extend the application of *in-situ* radiography and provide more detailed information concerning foam formation.

For instance, the stability of metal foams has mainly been studied *ex situ*, *i.e.* the foaming process was interrupted at some point and then the structures of (different) solidified samples were analyzed. In a next step, synchrotron radiation allowed the observation of foam formation and decay for individual samples *in situ* by radiography [1–4].

In this work, *in-situ* x-ray radiography was combined with image processing to investigate foam stability and expansion during foam formation. Foam stability was characterized by the definition of a quantitative measure for *coalescence events*. We develop a procedure which calculates this measure from a sequence of 2d projected radiographs. In a particular application, the influence of silicon-carbide particles of different size on foam stability was studied.

Using algorithms for velocity field computation known from computer vision, we perform the estimation of *local expansion rates*. It gives an opportunity to draw conclusions concerning distribution of expansion forces *inside* foaming metals.

2. EXPERIMENTAL SET-UP

A sketch of the experimental set-up for the investigation of metal foams is schematically depicted in Fig. 1. The essential parts there are the sample, x-ray source, furnace and detector. The furnace is additionally equipped with two aluminium windows, which are transparent for the x rays. During sample melting and foaming, the photons emitted by the x-ray source pass through the sample and are counted by the digital detector system, *e.g.* based on a charge-coupled device.

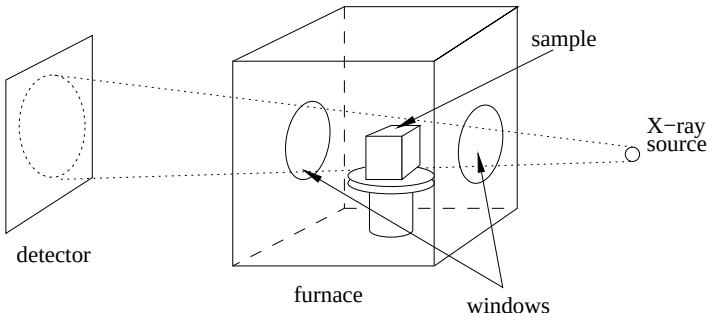

Figure 1. Outline of the experimental radiography set-up.

The acquired radiograph is a 2d array S of size $M \times N$. For monochromatic radiation the signal magnitude at pixel (i, j) is

$$S(i,j) = \int_{\Delta t} \left[\int_{\Delta y} \int_{\Delta x} \underbrace{I_0 e^{-\int_z \mu(x,y,z,t)dz}}_{I_T(x,y,t)} dxdy \right] dt,$$

where I_0 and I_T correspond to incident and transmitted intensities, $\mu(x, y, z, t)$ is the spatial distribution of the linear attenuation coefficient at the chosen x-ray energy, Δx and Δy are lateral detector pixel sizes, *i.e. sampling distances*, and Δt is the time between two successive exposures or *sampling time*.

In our work, the radiograph sequences were produced employing synchrotron light at beamline ID19 of the European synchrotron ESRF. A monochromatic synchrotron x-ray beam (33 keV) is used for the acquisition of radiographic image sequences (pixel sizes from 40 μm down to 1 μm) with frame rates ranging from 2 to 18 s^{-1}, as previously described in more detail [4].

3. IMAGE ANALYSIS

3.1. Estimation of coalescence rates

Spontaneous ruptures of liquid films and further merging of several pores into a larger one is commonly called *coalescence*. The observation of such an event by x-ray radiography is presented in Fig. 2. Together with the *drainage* effect, *i.e.* motion of liquid under gravity through the foam structure, coalescence plays an important role for foam decay. The investigation of the coalescence process allows one to draw conclusions concerning foam *stability*, which is defined as the foam's ability to keep its structural and mechanical properties unchanged during a prolonged temporal period.

Work has been performed on the development of theoretical models for drainage and coalescence effects [8, 9]. However, verification and refinement of these models demand additional experimental investigation.

The sampling theorem [10], well-known from signal processing, establishes a minimal *sampling time* Δt, *i.e.* the time between two successive radiograph exposures, to follow a continuous process from one frame to the other without information losses. In the case of metal foams, foaming could be considered as superposition of parallel processes running with different velocities. There are slow processes (*e.g.* pore inflation and movement, foam expansion)

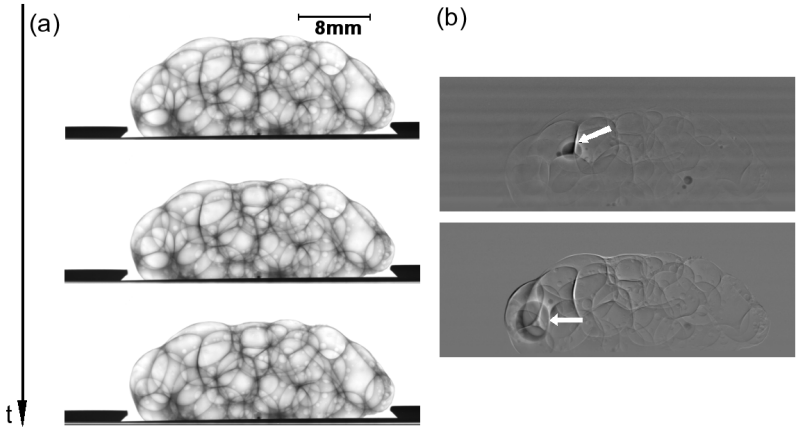

Figure 2. Examples of metal films ruptures , *i.e.* coalescence events (pointed by white arrows), where (a) image sequence of metal foaming (d) difference image of successive frame .

and discontinuous, abrupt ones (*e.g.* films ruptures which are fast [3, 4]). We adapt the experimental conditions in such a way that slow processes are followed and coalescence breaks the sampling condition. Consequently, coalescence events are declared as events violating the sampling theorem.

For a radiograph sequence of N images taken at times $t_i = i\Delta t$ where $i \in \{0, 1, ..., N-1\}$, we introduce the following measures to quantify the coalescence process:

- the *coalescence rate* $a(t_i) = a_i = d_{i,i+1}/\Delta t$ is the event area density $d_{i,i+1}$ (*i.e.* the summed projected area of detected events between frames i and $i+1$ normalized to the total image area) per sampling time.
- the effective *integral coalescence* $A(t_i)$ is defined as the total area density of the events over the time interval $[0, t_i]$: $A(t_i) = A_i = \Delta t \sum_0^i a_i$.

We developed a procedure for detecting and measuring coalescence events based on signal processing in Fourier domain. For two given successive images of a radiograph sequence S_i, S_{i+1} we apply an algorithm based on recursive image partitioning. According to the shift theorem [10], signal shifting in the spatial domain has no impact on the amplitude spectra, instead the phase of the transformed signal is altered. Thus, if the difference between amplitude spectra of partitions of two successive frames is inferior to a predefined threshold T_ε, then only local signal displacement took place and therefore it could be discarded from further analysis. Otherwise the partition is further divided (*i.e.* down to a predefined smallest partition size) and the resulting sub-partitions reevaluated as above. The event area density $d_{i,i+1}$ is obtained by summing the areas of these smallest partitions normalized to the image area. Finally, the coalescence rate $a(t)$ and integral coalescence $A(t)$ are calculated as previously defined.

In order to test the developed procedure a simulation approach was used. For this we empoyed the so-called *isolated soap bubble model* where collapses of bubbles are simulated in a three-dimensional (3D) volume using a ray-tracing algorithm [11] and a subsequent estimation of coalescence rates from calculated projected radiographs. The model consist of N bubbles enclosed in a 3d volume. The bubbles are rising and at some point can burst and disappear, see

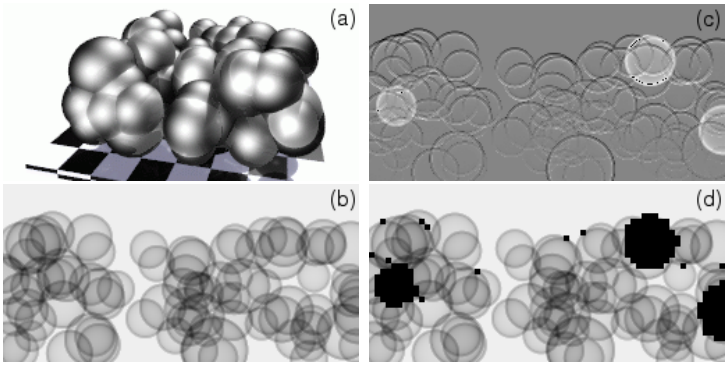

Figure 3. Model of isolated soap bubbles: (a) 3D scene (b) simulated radiograph (c) difference of successive frames (d) events detected by the developed image analysis.

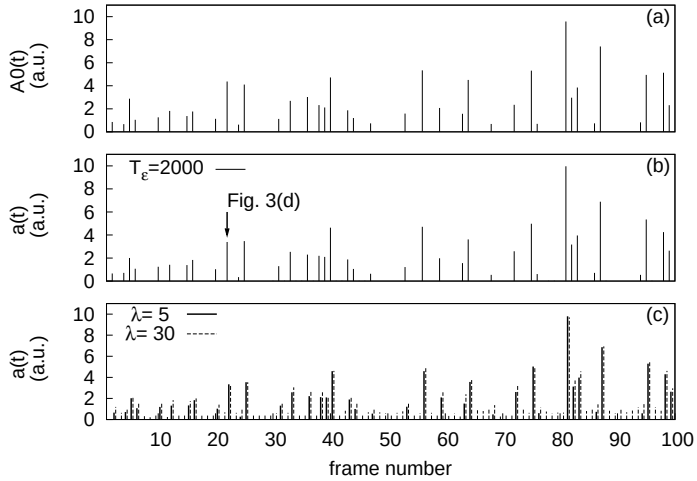

Figure 4. (a) Original events are projected area of collapsed bubbles $A_0(t)$ versus (b) coalescence rate $a(t)$ for a chosen threshold T_ε, where arrow points to the moment presented by Fig. 3(d). (c) Influence of Poisson noise of different strength ($\lambda = 5, 30$) on coalescence rate measurements.

Fig. 3. The model parameters are a bubble ensemble $B = \{b_0, b_1, ..., b_N\}$, velocities describing rising (v_y) and bubble growth (v_R), and a coalescence policy function $P_C : t \rightarrow i$, stating that bubble $b_i \in B$ disappears at time t.

Simulation results are presented in Fig. 4. As original events we chose the calculated projected area of collapsed bubbles, see Fig. 4 (a), which is compared with the coalescence rate $a(t)$ determined by our image analysis on the projection image sequence, Fig. 4 (b). We see, that the positions and magnitudes of coalescence events are well reproduced by evaluation of the projection image sequence.

Additionally, we tested the algorithm's robustness with respect to image noise. The original image sequences were intentionally corrupted by Poisson noise of different strength. Pixel intensities are recomputed as

$$\hat{S}(i,j) = S(i,j) + n(i,j)$$

where the noise value $n(i,j)$ is distributed by the Poisson probability mass function $P_\lambda(x) = \frac{e^{-\lambda}\lambda^x}{x!}$ and λ is the mean and variance of the distribution. Fig. 4(c) shows coalescence rates $a(t)$ estimated from the corrupted image sequence. In the case $\lambda = 30$ one recognizes small

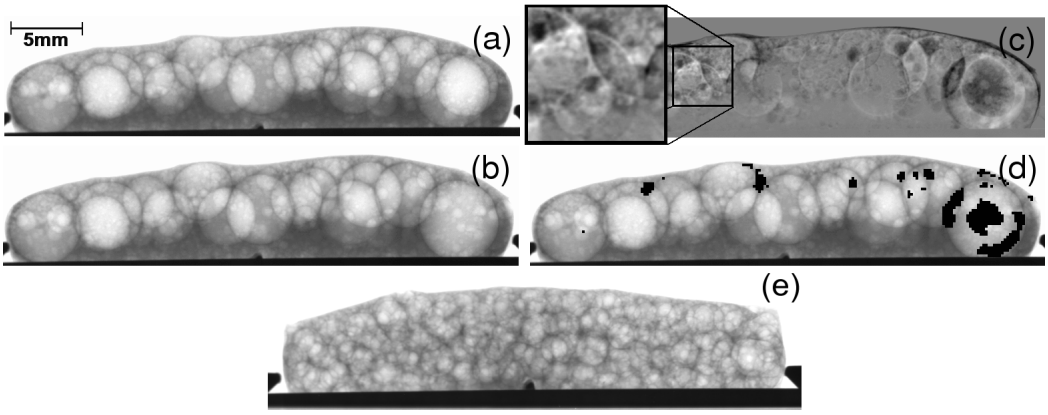

Figure 5. Collapse of metal films leading to coalescence of various bubbles detected by real-time radiography in two successive frames (a) and (b) of sample A (SiC particles of size 63 μ). The difference image with enlarged region(c) highlights the changes between the two frames. Image analysis yields the marked events as black regions in (d). Radiography of sample B (SiC particles of size 3 μ) at the same foaming time in (e).

artefacts which appear due to the strong noise level. Still as before we see significant correlation between original (a) and detected (c) events, especially for such of high magnitude.

The developed method was applied to radiographic image sequences of foaming metals. Foam samples were produced by the so-called FORMGRIP process [12] which consists of the production of a precursor material and foaming under heat treatment. The latter was in our case performed with simultaneous real-time radiography.

In the precursor preparation stage, a gas-releasing blowing agent (TiH_x) was mixed into a re-melted metal matrix composite (MMC) by mechanical stirring and subsequently cooled to far below the solidification temperature. MMCs (AlSi9Mg0.5/10vol%SiC_p) with different sizes of silicon-carbide particles (SiC) were used.

In the following, samples of the resulting precursor materials were baked in a furnace. This was pre-heated to a temperature of $\approx 725\,^\circ$C, *i.e.* well above the liquidus temperature ($\approx 600\,^\circ$C) in order to achieve a high sample heating rate.

As an example we present details on two samples of size $30 \times 3 \times 6$ mm^3, one with SiC particles of mean diameter $\bar{D} = 63$ μm (sample A), the other with $\bar{D} = 3$ μm (sample B). In Fig. 5, two successive frames [(a) and (b)] of the image sequence are shown for sample A. The difference image (c) shows appearing liquid in darker grey and vanishing liquid (mostly metal films) in lighter grey than the background. The black regions marked on (d) correspond to the detected coalescence events obtained by the developed image analysis.

Results for the two samples are subsumed in Fig. 6, *i.e.* the temporal evolution of temperature measured by thermocouples within the sample, foam expansion (a) and coalescence rates $a(t)$ and $A(t)$ (b, c), where additionally a running average $\langle a \rangle(t)$, *i.e.*

$$\langle a \rangle(t) = \frac{1}{T} \int_{t-T/2}^{t+T/2} a(\tau) d\tau$$

over the time window $T = 25$ s is plotted. The temperature evolution of Fig. 6 (a) shows

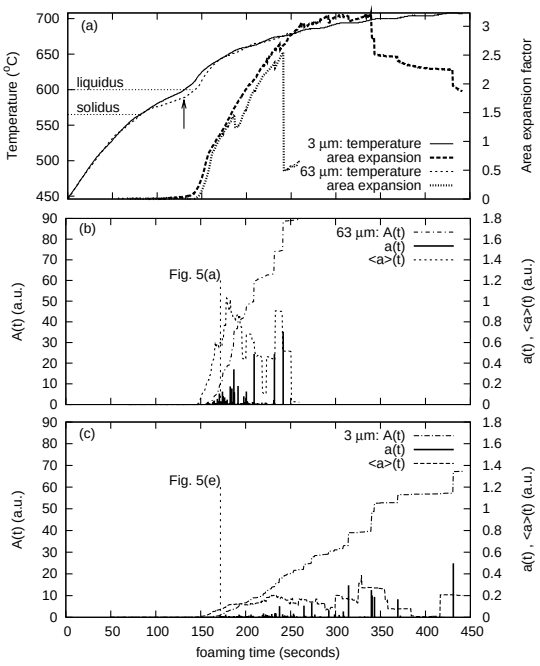

Figure 6. Temperature and computed area expansion (a) and coalescence measures of two samples with different mean sizes $\bar{D}$ of SiC particles, for sample A with $\bar{D} = 63$ μm (b) and for sample B with $\bar{D} = 3$ μm (c) ($T_\varepsilon = 9000$).

a comparable heating rate in the two samples. The area expansion curves are similar to the expansion observed by *in-situ* optical methods investigating the external shape of the foam, *e.g.* as obtained by laser-based expandometers described in the following section. Evidently, expansion starts roughly where the transition to the liquid state occurs (see arrow marking the temperature dips corresponding to the latent heat of fusion). The expansion curves suggest a similar foaming behaviour of the two samples in the first stage up to $t \approx 240$ s.

In contrast, *in-situ* radiography of both samples, see Fig. 5 (a,e), and the measured coalescence reveal significant differences between the two samples, see plots of Fig. 6 (b, c). The coalescence rates $a(t)$ indicate differences in the evolution of the internal foam structures.

For both samples, already soon after the onset of foam expansion, first coalescence events are detected by the coalescence rate $a(t)$. They have a low amplitude corresponding to a small radiographic projection area. With proceeding foaming time the events tend to get less frequent but higher in amplitude due the fact that pores tend to be larger. Therefore, at late stages, individual film rupture events have higher impact on the foam structure which in some cases even changes the external shape.

Comparing the two samples we notice that sample A exhibits a higher coalescence rate than sample B, especially at the very beginning. The increased slope of the integral coalescence $A(t)$ indicates that already during early foam expansion a higher fraction of liquid metal films collapses. According to the radiographs of sample A in states of high expansion (factors from 1 up to $\approx$2.5 in Fig. 6 (a), *i.e.* at similar expansion stages to sample B) the foam structure is rather coarse. Both, the increased coalescence rate and the observation of a coarse structure in the radiographs in presence of large particles lead to the conclusion that those metal films tend to collapse at increased thickness compared to melts prepared with small particles. These

findings support the hypothesis that, when liquid films thin down to the thickness of solid particles in the melt, the metal films recede from the particles [1] under unfavorable wetting conditions.

3.2. Estimation of local expansion velocities and rates

Previously, Duarte and Banhart have shown [13] an approach for the *in-situ* study of metal foams. They used an "expandometer" [14] which is a device equipped with a laser sensor, measuring the displacement of the foam front during metal foaming. In their work the expansion behaviour was compared for different experimental conditions and precursor materials such as alloy composition, pressing parameters, foaming temperature or heating rate.

X-ray radiography combined with image analysis has several advantages over the method presented above. First of all, radiography offers an information about internal sample structure during foaming. Application of automated image analysis on a 2d radiograph sequence allows the computation of quantitative properties related to metal foam structure and its evolution. It can not only help to analyze a displacement of external foam shape, but also allows us to investigate material flows *inside* foaming samples which would highlight additional aspects about expansion forces and their distribution, and, consequently, about metal foaming processes in general.

The velocity field determination, also known as *optical flow* computation, is one of the fundamental problems in image vision, already formulated by Horn and Schunk [15] in 1981. A good survey of now existing techniques can be found in Ref [16] .

One particular algorithm takes as input a sequence of 2d radiographic projection images and calculates a velocity map $v(x, y, t)$. Each vector is composed of a vertical and a horizontal component, *i.e.* $v = (v_x, v_y)$. Since the gravitational force is acting along the vertical direction (*i.e.* parallel with respect to foam expansion), the statistical characteristics of the foaming process on the same vertical level are expected to be the same. This allows us to estimate a vertical velocity component $\bar{v}_y$ averaged over an image width $w_x = M\Delta x$, *i.e.*

$$\bar{v}_y(y,t) = \frac{1}{w_x}\int_0^{w_x} v_y(x,y,t)dx$$

We introduce a *local expansion rate*

$$F(y,t) = \frac{\partial \bar{v}(y,t)}{\partial y},$$

which can be understood as velocity gradient in the vertical direction. The discrete case is implemented by

$$F(j,k) = \left(\bar{v}(j - \Delta s/2, k) - \bar{v}(j + \Delta s/2, k)\right)/\Delta s,$$

where Δs is vertical size of the employed differentiation window.

The evaluation of the velocity maps and local expansion rates enables the investigation of the temporal uniformity of the foaming process. For example, for one particular sample of $17 \times 5 \times 6$ mm^3 size composed of AlSi7 alloy mixed with 0.5 wt.-% TiH_2 powder as blowing agent and foamed at a temperature of $\approx 725\,^{\circ}\mathrm{C}$, a two-stage expansion phase was noticed from

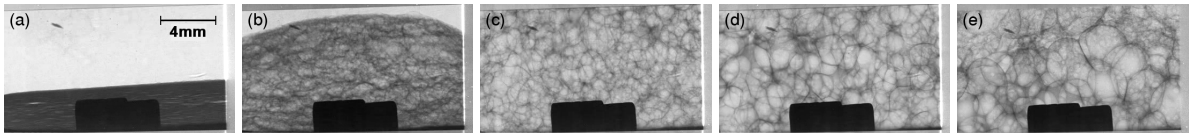

Figure 7. Selected frames of a radiography sequence of a foamed AlSi7 sample: 50 sec (a), 100 sec (b), 150 sec (c), 200 sec (d) and 400 sec (e). The entire radiograph sequence consist of 400 images with 40 μm pixel size taken with a frame rate of $\approx$ 1 Hz.

the radiograph sequence (see selected frames at different expansion stages in Fig. 7): the foam sample approaching the melting temperature of the alloy starts to expand very rapidly. After reaching a certain height its expansion comes to a halt for a short time. Later, it continues its growth, with accelerating expansion again.

This behaviour can be analysed quantitatively by the measures defined above. The 2d plot of Fig. 8 (a) represents a velocity map $v_y(y,t)$ as a function of vertical position y and foaming time t. For this particular uniaxially compacted sample (expanding mainly in the vertical direction [1]), a vertical cut through the plot at 80 sec, cf. Fig. 8 (b), shows that the upper foam layers are growing with higher velocities in comparison with lower ones (since the upper layers are displaced by expansion of the lower layers and themselves are expanding at the same time). Another cut, taken horizontally from (a) at $y = 100$, illustrates a particular velocity distribution during foaming, see Fig. 8 (c): the two distinct expansion stages seen from the radiographic sequence are reflected by two velocity peaks at foaming times 50 and 90 seconds.

Examining the distributions of local expansion rates, Fig. 8 (d), we observe light tracks. They correspond to the fast expansion of large bubbles which are rising due to ongoing pore inflation underneath. Again we observe a two-stage expansion: the first expansion period from 35 sec to 60 sec, largely reduced expansion rates up to 75 sec, and the second expansion period from 75 sec onwards. The strong dark-light contrasts from 80 sec onwards stem mainly from pore coalescence.

These two stages of foam expansion are in agreement with studies of the decomposition behaviour of the TiH_2 blowing agent [17, 18]. The authors showed that TiH_2 powder without prior heat treatment exhibits two decomposition peaks. Our results could be interpreted as an effect of the two stages of gas release from the blowing agent.

4. SUMMARY

In summary, measures were defined to quantify mechanisms influencing the metal foaming process from sequences of projection images. Coalescence was quantified in order to investigate foam decay. Local velocities allow us to characterize foam expansion.

An image processing procedure was developed to determine coalescence rates and was applied to synchrotron radiography. The reported results give evidence of considerably different foam stability of metal melts with varying mean SiC particle sizes even if macroscopic expansion is similar. Comparing particle sizes of 3 and 63 μm, for the latter only a rather poor foam quality with a few large pores can be achieved owing to a considerably reduced stability of films involving a bad foamability.

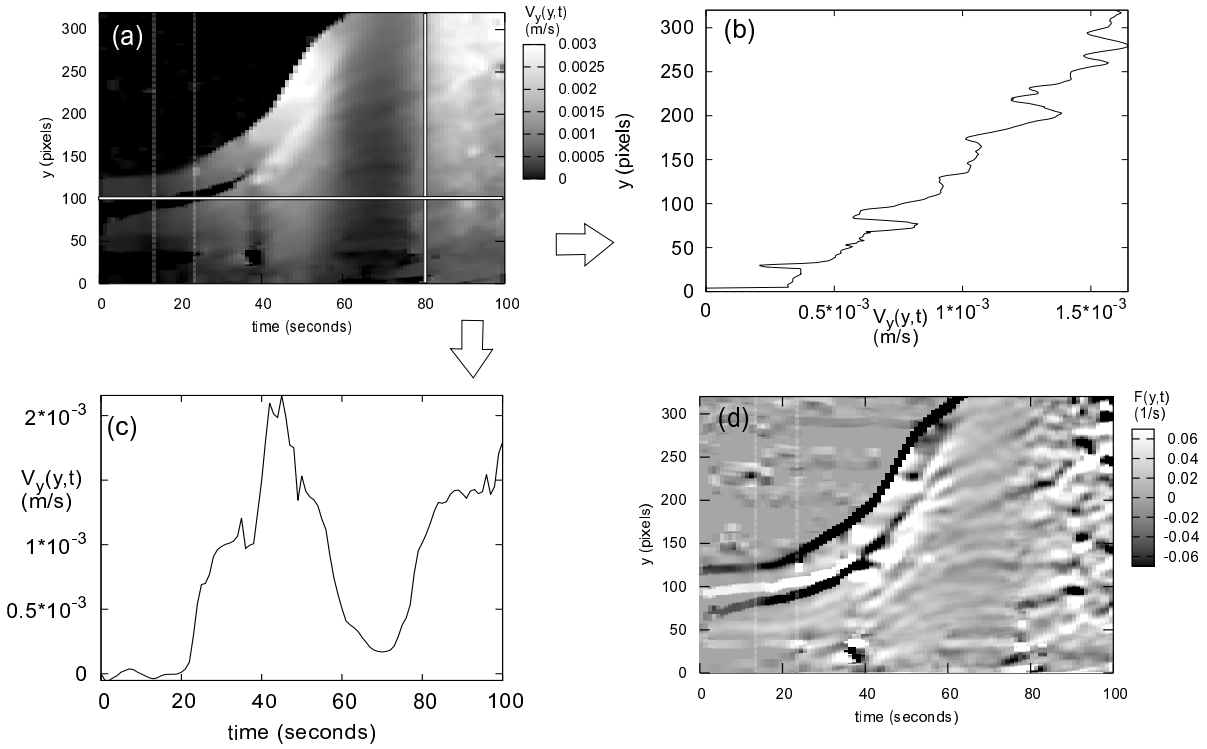

Figure 8. (a) Measured average growth velocity $\bar{v}_y(y,t)$ with two section along vertical (b) and temporal (c) axes. Distribution of local expansion rates $F(y,t)$ (d).

A calculation of optical flow from radiograph sequences offers an estimation of the local expansion rates during foam formation. It provides us with information about material flow inside metal foams and offers an opportunity to analyze foaming processes from a novel point of view. In addition to the quantitative investigation of expansion in general, the local expansion rates are able to show non-uniformities in the chosen samples, *i.e.* regions with strong local expansion and such with reduced expansion rates.

REFERENCES

1. J. Banhart, H. Stanzick, L. Helfen, and T. Baumbach. Metal foam evolution studied by synchrotron radioscopy. *Appl. Phys. Lett.*, 78:1152–1154, 2001.
2. J. Banhart, H. Stanzick, L. Helfen, T. Baumbach, and K. Nijhof. Real-time x-ray investigation of aluminium foam sandwich production. *Adv. Eng. Mater.*, 3:407, 2001.
3. H. Stanzick, M. Wichmann, Jörg Weise, L. Helfen, T. Baumbach, and J. Banhart. Process control in aluminium foam production using real-time x-ray radioscopy. *Adv. Eng. Mater.*, 4(10):814–823, 2002.
4. L. Helfen, H. Stanzick, J. Ohser, K. Schladitz, P. Pernot, J. Banhart, and T. Baumbach. Investigation of the foaming process of metals by synchrotron-radiation imaging. In N. Meyendorf, G.Y. Baaklini, and B. Michel, editors, *Proceedings SPIE: Testing, Reliability, and Application of Micro- and Nanomaterial Systems*, volume 5045, pages 254–265 (in press), 2003.
5. F. Garcia Moreno, M. Fromme, and J. Banhart. Real-time x-ray radioscopy on metallic foams using a compact micro-focus source. *Advanced Engineering Materials*, 6:416–420, 2004.
6. J. Banhart. Manufacture, characterisation and application of cellular metals and metal foams. *Progr. Mater. Sci.*, 46:559–632, 2001.

7. J. Banhart. Aluminium foams for lighter vehicles. *International Journal of Vehicle Design*, 37:114–125, 2005.
8. A. Bhakta and E. Ruckenstein. Drainage and coalescence in standing foams. *J. Colloid Interface Sc.*, 191:184201, 1997.
9. V. Gergely and T.W. Clyne. Drainage in standing liquid metal foams: modelling and experimental observations. *Acta Materialia*, 52:3047–3058, 2004.
10. B. Jähne. *Digital Image Processing.* Springer, 2002.
11. P. Mikulík, A. Myagotin, L. Helfen, and T. Baumbach. A simulation tool for evaluation of three-dimensional synchrotron-radiation and laboratory imaging using arbitrary scanning geometries. to be published.
12. V. Gergely and T.W. Clyne. The formgrip process: Foaming of reinforced metals by gas release in precursors. *Adv. Eng. Mater.*, 2:175–178, 2000.
13. I. Duarte and J. Banhart. A study of aluminium foam formation - kinetics and microstructure. *Acta Materialia*, 48:2349–2362, 2000.
14. P. Weigand. *Untersuchung der Einflussfaktoren auf die pulvermetallurgische Herstellung von Aluminiumschaum*. PhD thesis, RWTH Aachen, Aachen, Germany, 1999.
15. B. Horn and B. Schunck. Determining optical flow. *Artificial Intelligence*, 17:185–203, 1981.
16. S.S. Beauchemin and J.L. Barron. The computation of optical flow. *ACM Comput. Surv.*, 27(3):433–466, 1995.
17. B. Matijasevic, S. Fiechter, I. Zizak, N. Wanderka, P. Schubert-Bischoff, and J. Banhart. Decomposition behaviour of as-received and oxidized TiH_2 powder. In *PM 2004 17-21 October 2004, Vienna (Austria)*, 2004.
18. B. Matijasevic and J. Banhart. Improvement of aluminium foam technology by tailoring of blowing agent. *Scripta Materialia (in press)*, 2005.